2.3 ESTIMATES OF THE THOUGH THICKNESS RESIDUAL STRESSES IN THE AS-PROCESSED NFA-1 PLATE BASED ON NANOINDENTATION MEASUREMENTS—S. Pal, M. E. Alam and G. R. Odette (UCSB)

OBJECTIVE: The aim of the present study is to quantify the residual stresses that develop in deformation processed NFA-1 plate using a simple nanoindentation technique.

SUMMARY

Hardness and modulus of the as processed NFA-1 alloy plate have been measured using nanoindentations, including to probe the nature and magnitude of the residual stresses generated by thermo-mechanical processing. The residual stresses were quantified from the nanoindentation load-penetration curves. The plate surfaces (and adjoining mild steel can) are in compression, while the middle of the plate is in tension. The magnitude of the maximum tensile residual stress is ≈ +500 MPa, decreasing to ≈ +75 MPa near to the plate surface; and ≈ -30 MPa at the surface of the can. A microcrack population area density, lying perpendicular to the short thickness direction of the plate, tracks the residual tensile stress profile. The surface residual stresses were further quantified using a conventional $\sin^2\psi$ x-ray diffraction (XRD) method that yielded a value similar to the nanoindentation estimate.

PROGRESS AND STATUS:

Introduction

Nanostructured ferritic alloys (NFAs) are an attractive structural material for advanced nuclear fission and fusion applications due to their unique radiation tolerance, high-temperature strength, high fracture toughness and remarkably low value of the brittle to ductile transition [1,2]. However, bulk processing of NFA is extremely difficult due to a highly anisotropic α-fiber texture [3]. UCSB has collaborated with LANL and ORNL to develop a large heat NFA 14YWT variant called FCRD NFA-1. The extruded and cross rolled NFA-1 plate contains a large population of microcracks lying perpendicular to the short thickness direction, which runs in the primary deformation directions. Our previous investigation showed that during high-temperature thermo-mechanical processing, stress concentrations develop ahead of the dislocation pile-ups at {001}<110>-type low angle tilt boundaries. The tilt boundaries are composed of sessile <001> dislocations formed by reactions between two <111> dislocations gliding on {110} planes. The dislocation pile-ups lead to high-stress concentrations, and the summed Burger's vectors can directly nucleate a nano-scale crack. The {001}<110> boundary is also a low toughness brittle cleavage system for the crack nuclei. Thus residual stresses, that develop during thermo-mechanical processing, drive nano-to-micro cleavage crack propagation. The presence of residual stresses in the cracked region was previously qualitatively shown using selected area diffraction, by streaking of the diffraction spots [3]. Therefore, it is critically important to better quantify the residual stresses. Here, we use a simple nanoindentation technique to estimate the residual stresses based on a method proposed by Suresh et.al [5], as well as using a standard XRD $\sin^2\Psi$ method applied to the top surface of the canned plate. We show that the though-thickness microcrack density variation approximately tracks the residual stress profile.

Materials and Methods

A larger NFA heat, called FCRD-NFA-1, containing 14Cr-3W-0.4Ti-0.3Y and balance Fe was studied. NFA-1 was developed in a close collaboration between UCSB, LANL, and ORNL. NFA-1 was consolidated by hot extrusion at 850°C, then annealed, and hot cross-rolled at 1000°C perpendicular to the extrusion direction to a final plate plus can thickness of 12.5 mm.

The nanohardness (NH) and reduced modulus (E_r) of the as processed NFA- plate were measured using a nanoindenter (Hysitron, Tribo-indenter). Depth sensing instrumented nanoindentation provides a load versus penetration P-h curve. The P-h curve not only characterizes the NH and E_r, but can also provide information on strain hardening, creep, bi-axial residual stresses and yield strength. Here we evaluate the

bi-axial residual stresses present in the as processed NFA-1 alloy following the methodology proposed by Suresh et al. [5].

Figure1 shows a typical nanoindentation P-h curve obtained, where h_f is the final plastic depth and h_{max} is the maximum depth of penetration. The method of calculating hardness and modulus of a material from the P-h curve was first proposed by Oliver and Pharr [6].

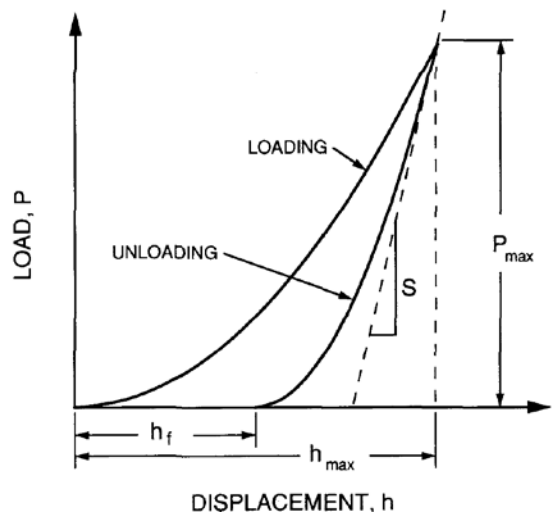

Figure 1. Schematic illustration of a typical nanoindentation load-displacement (P-h) curve.

The reduced Young modulus (E_r) of an indented substrate is related to the slope (S) of the initial unloading P-h curve and the contact area (A_r) between the indenter and the indented material as:

$$S = \frac{dP}{dh} = \frac{2}{\sqrt{\pi}} * \sqrt{A_r} * E_r \tag{1}$$

The reduced modulus, E_r, is given by,

$$\frac{1}{E_r} = \frac{1-\nu^2}{E} + \frac{1-\nu_i^2}{E_i} \tag{2}$$

Here the E and E_i are the Young moduli of the indented and indenter, and ν and ν_i are the Poisson ratios of the indented and indenter, respectively. The slope of the unloading portion of the load-displacement curve is determined by least squares fitting:

$$P = A(h - h_f)^m \tag{3}$$

Typical values of m fall in the range of 1.2 to 1.6, depending upon the material. Therefore, we have considered only those load-displacement curves with m in that range. The NH is the average contact pressure at the maximum load, defined by,

$$H = \frac{P_{\max}}{A_r} \tag{4}$$

If the indentation region is subjected to an equi-biaxial residual stress, the shape P-h curve is modified relative to a stress-free case as illustrated in Figure 2.

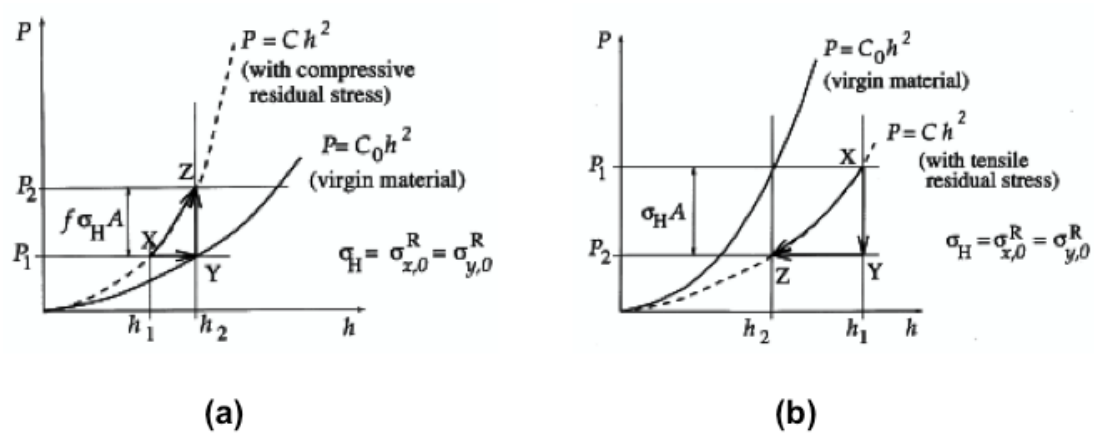

Figure 2. Schematic illustration of the P-h curves of unstressed (virgin) material and for compressive (a) and tensile (b) residual stresses [5].

The basic physics of the modification of the P-h loading curves is easy to understand as illustrated in Figure 3. If the region is under compression it takes a higher load, P, to produce a given indentation depth, while P is lower in the case of a tensile stress. Expressions describing the effect of residual stress on the curvature of the load-displacement curve, expressed in terms of the average contact pressure and area (hardness), were derived by Suresh et. al [5].

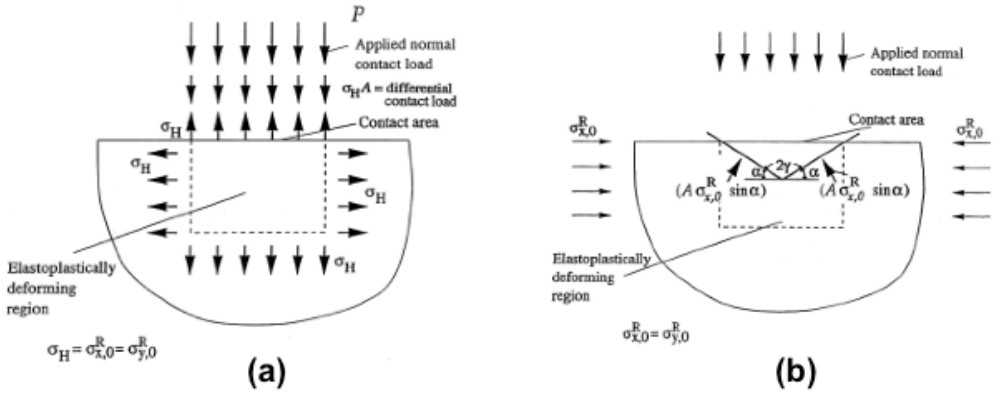

Figure 3. Schematic illustrations of the role of elastic residual stresses at the indented surface that are: a) tensile; and, b) compressive [5].

The hardness of a material defines its ability to resist plastic deformation. For a sharp indenter, the amount of plastic strain is not affected by pre-existing elastic residual stress. However, for an elastoplastic material, the apparent contact area changes in the presence of a residual stress. For a specified indentation depth, a tensile residual stress adds a hydrostatic stress component, σ_H, to the indentation stress tensor, including a component in the loading direction. The same hydrostatic stress is subtracted in the case of constant load indentation. Similarly, compressive residual stress can either add or subtract a hydrostatic stress component, $\sigma_H \sin\alpha$, along the direction of indentation. How an elastic bi-axial residual stress on the indented surface is equivalent to either tensile or compressive hydrostatic stress component is illustrated in Figure 3. Therefore based on the equivalence of the mean contact pressure and the relation between apparent contact area, residual contact stress and mean contact pressure was

established. The change in contact area due to elastic residual stress is related to mean contact pressure as:

$$\frac{A_r}{A_0} = \left(1 - \frac{\sigma_H}{P_{ave}}\right)^{-1} \quad \text{for a tensile residual stress} \tag{5}$$

$$\frac{A_r}{A_0} = \left(1 - \frac{\sigma_H \sin\alpha}{P_{ave}}\right)^{-1} \quad \text{for a compressive residual stress} \tag{6}$$

Here, α is the semi-apex angle of the indenter. For the sharp Berkovich indenter α = 24.8°, A_0 is the contact area between the indenter for a residual stress-free condition, and P_{ave} is the corresponding average contact pressure, or hardness [5].

Through thickness microstructural characterization of the NFA-1 plate at different plate views were carried out using FIB-SEM (Helios600, FEI), and has been reported previously [7]. Residual stress measurements using XRD were also carried out in a two-axis goniometer instrument (XPertPro, PAN-Analytical) using CuKα radiation. The (112) planes, with a peak in bcc Fe occur at 2θ = 83.219°, was chosen to measure changes in the lattice spacing, because of the higher sensitivity of the measurement at a large Bragg angles. Since the NFA-1 alloy has a strong texture, an initial θ-ω scan was performed to identify the ω angle with a maximum intensity for the (112) peak. The d-spacing measurements were performed using θ-2θ scan with a series of positive and negative ψ tilt.

Results

Figure 4 shows a schematic of the NFA-1 plate deformation directions. The residual stress profile developed in the short thickness direction of the plate was measured on a 45° cut section surface.

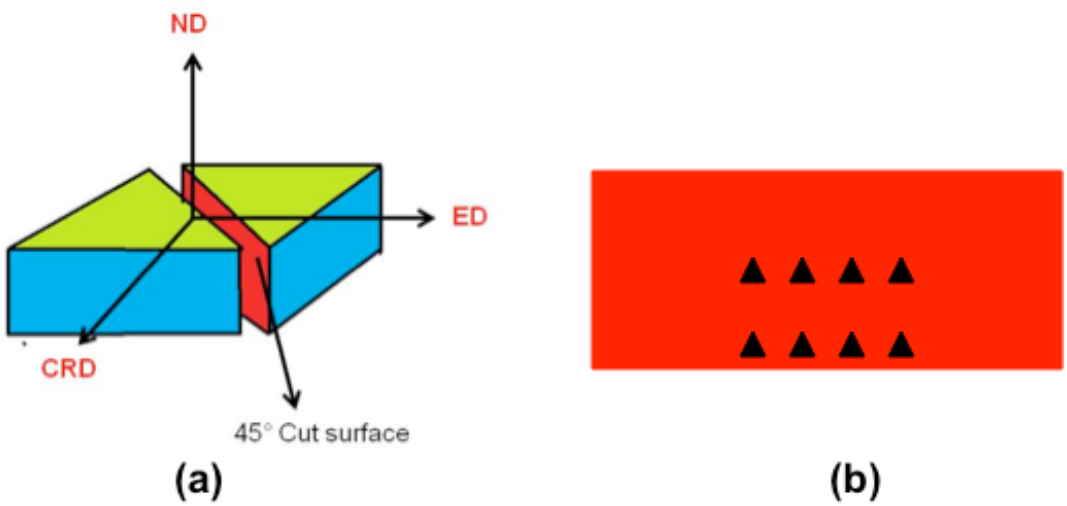

Figure 4. Schematic illustration of the: a) plate geometry and the deformation directions for the observed 45°cut plate section; and, b) the locations of nanoindentations for 45ºC surface.

Determination of the residual stress from the nanoindentation load-displacement curve requires a stress-free standard. Therefore a small rectangular specimen was cut from the thickness direction of the plate and annealed at 1000°C for 5h to relax the residual stresses present in the specimen. The standard sample was chosen from the thickness direction of the plate to maintain a microstructural and textural similarity between the stressed and standard stress-free specimens. The annealing condition was chosen

in such a way that it does not change in the microstructure of the specimen. It was previously reported that even a 32.4 kh treatment of a NFA alloy at 1000°C causes only minimal change in its microstructure [1]. Figure 5 displays the measured hardness and modulus of the 45° cut surface from the as-processed plate, and, 1000°C/5h annealed specimen which is used as a residual stress-free standard for the present case. The annealed specimen has the highest hardness, whereas the modulus remains same considering standard deviation. Variation in the hardness in the plate thickness occurs due to the presence of residual stress, whereas the magnitude of the residual stress also varies along the thickness. This affect the overall hardness of the 45°cut specimen, when it is measured from the different locations.

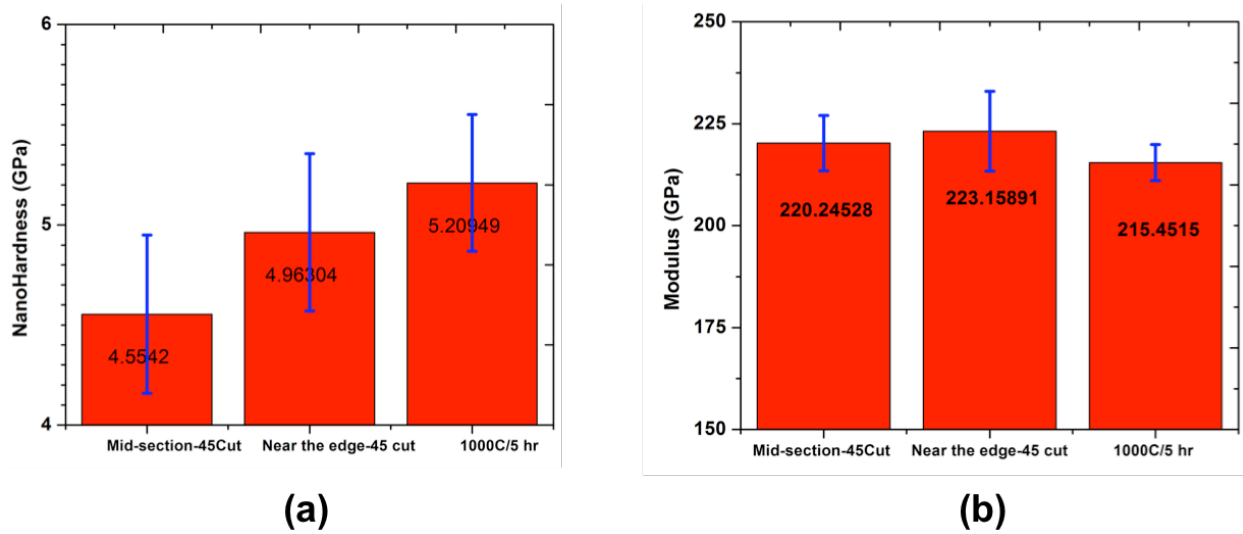

Figure 5. The NH (a) and E_r (b) for the different indent locations and specimen conditions.

Representative load-displacement curves for the three indented specimens are shown in Figure 6. The curvature of the loading portion of the load-displacement curve depends on the nature of the residual stress (compressive or tensile) in the indented region, again as described by Suresh et. al [5]. Clearly, the P-h curves are lower in the as-processed plate compared to the 1000°C/5 h heat-treated, nominally stress-free specimen. Therefore, the as-processed plate has a tensile residual stress profile in the thickness direction.

The curvatures of the loading P-h curve for the three indented specimens were least square fit using a generalized Kick's law [8], where the P is related to h as:

$$P = Ch^n \tag{7}$$

Here *C* reflects the magnitude of the loading curve and n is an empirical exponent that depends on the indenter geometry. The values for C and n are given in Table 1. The best-fit n is ≈ 1.65 in all three cases, consistent with significant strain hardening [9]. Equations 5 and 6 hold for n = 1.65, and the residual stress is given by Eq. 5. The contact areas and average contact pressures, or hardness values, were evaluated from the load-displacement curves shown in Figure 7. The curvatures of the loading portions of the P-h curves, determined by the second derivative of Eq. 7 at a fixed depth of 200 nm, are also given in Table 1. The estimated magnitudes of the residual stresses ranging from ≈ 500 MPa in the middle to ≈ 75 MPa near the plate edge. Note the plate is contained inside a can so it is expected that compressive residual stresses would exist near the canned plate surface.

These residual stress estimates are very approximate, but are consistent with results in the literature, for example for cold-rolled ferritic steel in Reference [10]. The residual tensile stresses drive microcrack propagation. And, notably, the estimated stress distribution crudely tracks the through thickness variation

of the microcrack density illustrated in the low magnification FIB-SEM images in Figure 8. Figure 9 shows the variation of the microcrack areal density in the plate thickness direction. The center of the plate is zero, and the distances from center of the plate to both edges are normalized by the plate thickness. The distribution is not symmetric, and peaks between the center and one of the edges of the plate. However, the middle half section of the plate has the highest crack density and the maximum residual tensile stress, whereas near to the plate edge both the crack density and the residual tensile stresses are lower.

The residual stresses in the top surface of the canned plate were also measured by the XRD $\sin^2\psi$ method [11] and found to range from ≈ -29 (compression) to +64 (tension). Details of this analysis will be reported in the future along with through-thickness measurements that are planned. The qualitative variation the residual stress is shown in Figure 10.

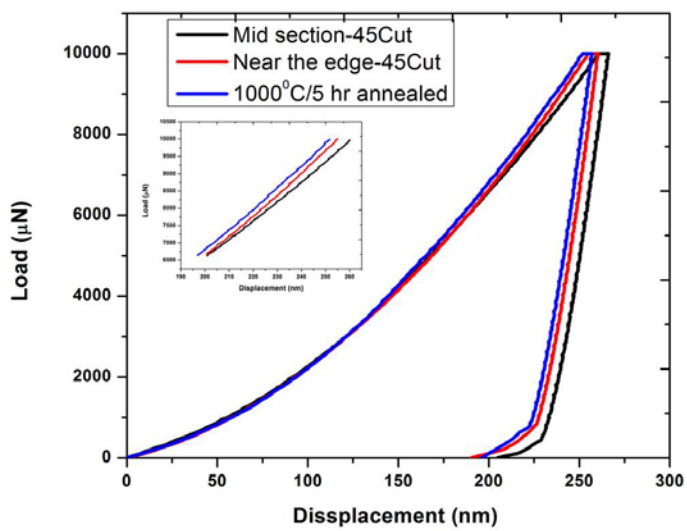

Figure 6. P-h curves obtained near the edge, and midsection of the cross-rolled plate section, as well as the 1000°C/5 h, annealed reference specimen. The inset shows a magnified view of the loading curve.

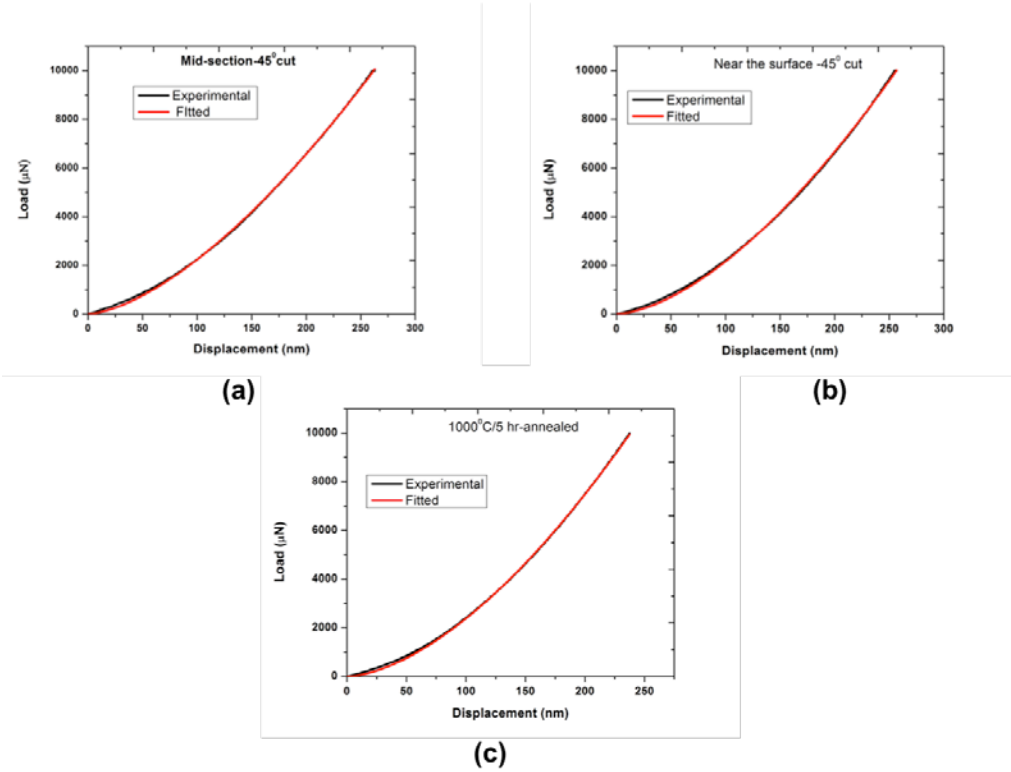

Figure 7. Least square fits to the loading indentation curves in Fig. 6: a) 1000°C/5 h; b) mid-plate; and, c) near edge.

Table 1. Least square fits of C, n, curvature of the loading portions (measured by taking double derivative of the curve at a fixed depth of 200 nm) and the corresponding estimated residual stress.

Locations /Conditions	C	n	Curvature @200 nm	Residual stress (MPa)
Mid-thickness	0.937	1.66	1.03	496
Near the edge	0.943	1.67	1.06	75
1000°C/5 hr	1.167	1.66	1.26	-

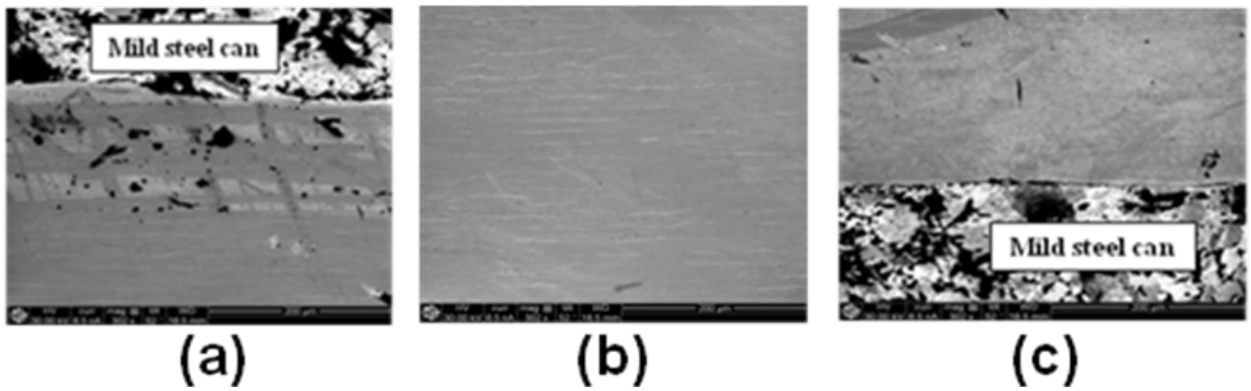

Figure 8. FIB-SEM low magnification micrographs of the of the plate thickness section: a) near the top edge; b) midsection; and, c) near the bottom edge. The mild steel can is clearly visible in the images.

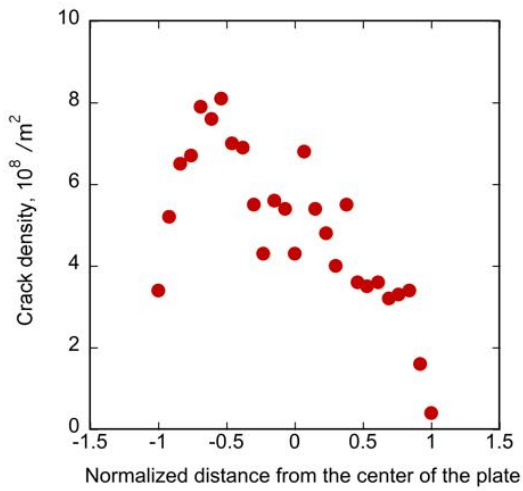

Figure 9. The crack areal density distribution profile through the plate thickness. The center of the plate is zero, and the distances from center of the plate to both edges are normalized by the plate thickness.

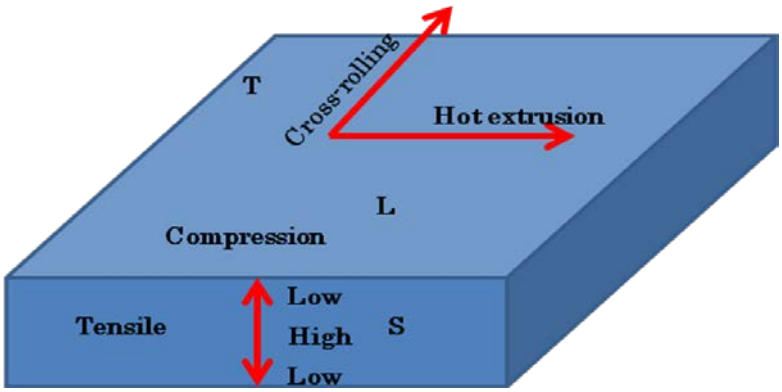

Figure 10. A schematic illustration of the NFA-1 plate showing the residual stress profiles along the different direction.

Summary and Discussion

We reported for the first estimates of the residual stress distribution in the as-processed NFA-1 plate. The results are qualitative and very approximate, but show robust trends. The mid-thickness region of the plate exhibits a very high tensile residual stress nominally ≈ +500 MPa, coincident with a very high micro-crack population area density. The residual tensile stresses near the edge of the canned plate are ≈ +75 MPa with a correspondingly low microcrack density. XRD techniques were used to characterize the stresses on the top surface of the canned plate that were also low and in one case compressive. Future residual stress measurements will be carried out at synchrotron x-ray and neutron facilities.

Acknowledgments

Acknowledge fusion, NEUP, LANL, and FCRD funding and the contributions of Hoelzer and Maloy in developing NFA-1.

References

[1] G. R. Odette, "Recent Progress in Developing and Qualifying Nanostructured Ferritic Alloys for Advanced Fission and Fusion Applications," *JOM,* vol. 66, pp. 2427-2441, 2014.
[2] M. E. Alam, N. J. Cunningham, D. Gragg, K. Fields, G. R. Odette, D. T. Hoelzer and S. A. Maloy, "Mechanical Properties Characterization of a Larger Best Practice Heat o f14YWT NFA-1," *Fusion Reactor Materials Program,* vol. 56, pp. 63-69, 30 June 2014.
[3] S. Pal, M.E. Alam, G. R. Odette, D. T. Hoelzer and S. A. Maloy (LANL) "Characterization of the Microstructure and Texture of NFA-1 for Two Deformation Processing Routes", *Fusion Reactor Materials Program*, Vol. 58, pp. 66-82, 30 June 2015.
[4] S. Pal, M.E. Alam, G. R. Odette, J. Lewandowski, D. T. Hoelzer and S. A. Maloy (LANL) "Characterization of the Microstructure and Texture of NFA-1 for Two Deformation Processing Routes", *Fusion Reactor Materials Program*, Vol. 58, pp. 29-41, 30 June 2015.
[5] S.Suresh, A.N. Giannakopoulus, "A new method of emstimating residual stress by instrumented sharp indenation", Acta Materialla, vol. 46, pp. 5755-5767, 1998.
[6] W.C.Oliver and G.M.Pharr, "An improved technique for determining the hardness and modulus using load and displacement sensing indentation experiments" J. Mater. Res., Vol. 7, 1564-1583, June 1992.

[7] M. E. Alam, S. Pal, D. Gragg, G. R. Odette, D. T. Hoelzer and S. A. Maloy, "Microstructural and Mechanical Behavior of As-Fabricated and Annealed 14YWT NFA-1 Alloy," *Fusion Reactor Materials Program,* vol. 59, December 31, 2015.

[8] F.Kick," Das Gesetz der proportionalen Widerstände und seine Anwendung auf Sanddruck und Sprengen" Dinglers Polytechnisches Journal, vol. 250, pp.141-145, 1983.

[9] S. V. Hainsworth, H. W. Chandler, and T. F. Page, "Analysis of the nanoindentation load-displacement curve" J. Mater. Res., Vol. 11, 1987-1995, August 1996.

[10] J.M. Atienza , M.L. Martinez-Perez , J. Ruiz-Hervias, F. Mompean , M. Garcia-Hernandez , M. Elices " Residual stress in cold drawn ferritic rods" Scripta Materialia, Vol. 52, pp. 305–309, 2005.

[11] C. Balasingh and A.K.Singh, "Residual stress and their measurements by X-ray diffraction methods" Metals, Materials and Processes, vol. 12, pp. 269-280, 2000.